0026-895X/08/7402-320–329$20.00
MOLECULAR PHARMACOLOGY
Vol. 74, No. 2
46458/3353442
Mol Pharmacol 74:320–329, 2008
Printed in U.S.A.

ACCELERATED COMMUNICATION

Targeted Disruption of Murine Organic Anion-Transporting Polypeptide 1b2 (oatp1b2/*Slco1b2*) Significantly Alters Disposition of Prototypical Drug Substrates Pravastatin and Rifampin

Hani Zaher, Henriette E. Meyer zu Schwabedissen, Rommel G. Tirona, Melissa L. Cox, Leslie A. Obert, Nidhi Agrawal, Joe Palandra, Jeffrey L. Stock, Richard B. Kim, and Joseph A. Ware

Pfizer Global Research and Development, Ann Arbor, Michigan (H.Z., J.P., M.L.C., L.A.O., N.A., J.A.W.) and Groton, Connecticut (J.L.S.); Division of Clinical Pharmacology, Department of Medicine, and Department of Physiology and Pharmacology, The University of Western Ontario, London, Ontario, Canada (H.E.M.z.S., R.G.T., R.B.K.); Lawson Health Research Institute, London, Ontario, Canada (R.B.K.)

Received February 18, 2008; accepted April 14, 2008

ABSTRACT

Organic anion-transporting polypeptides (OATP) 1B1 and 1B3 are widely acknowledged as important and rate-limiting to the hepatic uptake of many drugs in clinical use. Accordingly, to better understand the in vivo relevance of OATP1B transporters, targeted disruption of murine *Slco1b2* gene was carried out. It is noteworthy that *Slco1b2*(−/−) mice were fertile, developed normally, and exhibited no overt phenotypic abnormalities. We confirmed the loss of Oatp1b2 expression in liver using real-time polymerase chain reaction, Western Blot analysis, and immunohistochemistry. Expression of Oatp1a4 and Oatp2b1 but not Oatp1a1 was greater in female *Slco1b2*(−/−) mice, but expression of other non-OATP transporters did not significantly differ between wild-type and *Slco1b2*(−/−) male mice. Total bilirubin level was elevated by 2-fold in the *Slco1b2*(−/−) mice despite the fact that liver enzymes ALT and AST were normal. Pharmacological characterization was carried out using two prototypical substrates of human OATP1B1 and -1B3, rifampin and pravastatin. After a single intravenous dose of rifampin (1 mg/kg), a 1.7-fold increase in plasma area under the concentration-time curve (AUC) was observed, whereas the liver-to-plasma ratio was reduced by 5-fold, and nearly 8-fold when assessed at steady-state conditions after 24 h of continuous subcutaneous infusion in *Slco1b2*(−/−) mice. Likewise, continuous subcutaneous infusion at low (8 μg/h) or high (32 μg/h) dose rates of pravastatin resulted in a 4-fold lower liver-plasma ratio in the in *Slco1b2*(−/−) mice. This is the first report of altered drug disposition profile in the *Slco1b2* knockout mice and suggests the utility of this model for understanding the in vivo role of hepatic OATP transporters in drug disposition.

Carrier-mediated membrane transport is now widely appreciated as a critical determinant of drug uptake, distribution, and elimination (Ho and Kim, 2005). The organic anion-transporting polypeptide (OATP) transporters belong to a large family of membrane proteins that mediate the sodium-independent cellular uptake of a variety of amphipathic compounds, including hormones, bile acids, eicosanoids, environmental toxins, and many drugs in clinical use today (Tirona and Kim, 2007). Members of this family are expressed in a variety of organs of relevance to drug disposition or response, such as liver, kidney, brain, and intestine (Marzolini et al., 2004). One subset of the OATP transporters that has received

This work was supported in part by United States Public Health Service grant GM54724 (R.B.K.) and the Deutsche Forschungsgemeinschaft grant ME 3090/1-1 (H.E.M.z.S).

H.Z. and H.E.M.z.S. contributed equally to this work.

Article, publication date, and citation information can be found at http://molpharm.aspetjournals.org.
doi:10.1124/mol.108.046458.

ABBREVIATIONS: OATP/Oatp, organic anion-transporting polypeptide; ES, embryonic stem; bp, base pair(s); PCR, polymerase chain reaction; kb, kilobase pair(s); F, forward; R, reverse; FBS, fetal bovine serum; PBS, phosphate-buffered saline; TBS-T, Tris-buffered saline/Tween 20; LC-MS/MS liquid chromatography/tandem mass spectrometry; AUC, area under the concentration-time curve; SLC, solute carrier; V_{SS}, volume of distribution at steady state.

significant attention in relation to hepatic drug uptake is the human OATP1B subfamily. There are two members, OATP1B1 (*SLC21A6*, *OATP-C*, *OATP2*, *LST-1*) and OATP1B3 (*SLC21A8*, *OATP-8*, *LST-2*) in humans, which share 80% sequence homology (Hagenbuch and Meier, 2004). Both transporters have been described to be highly expressed in human liver (Abe et al., 1999, 2001; König et al., 2000; Ho et al., 2006) and are localized to the basolateral membrane, facilitating the hepatocellular uptake of endo- and xenobiotic substrates before their metabolism and efflux from the liver (Shimizu et al., 2005). In rodents, there is only one member of the Oatp1b subfamily. This transporter, termed oatp1b2 (*Slco1b2*, *Lst-1*, *oatp4*), has been identified in rat and mouse and is thought to be the closest ortholog of both human OATP1B1 and -1B3 (Cattori et al., 2000; Choudhuri et al., 2000; Ogura et al., 2000).

Although a number of in vitro and cell-based model systems for the study of OATP transporters exit, a murine *Slco* knockout mouse model has not yet been reported. The lack of such a model has prevented the delineation of the overall contribution of a given Oatp transporter to the organ-specific elimination of drugs shown to be substrates of multiple Oatp transporters in vitro.

Because the mouse genome contains only one S*lco1b* subfamily member, we hypothesized that the targeted disruption of this transporter should allow for a better delineation and extrapolation of the in vivo relevance of human OATP1B1 and OATP1B3 to the hepatic uptake of substrate drugs. Accordingly, we now report on the generation of a *Slco1b2* knockout mouse model. In addition to assessing the relative impact of this transporter to alterations of liver function or phenotype, we wanted to evaluate the utility of this model in terms of clarifying the relevance of Oatp1b2 in the hepatic elimination of prototypical substrates of human OATP1B1 and OATP1B3, such as rifampin and pravastatin. Indeed, studies from a number of laboratories, including ours, suggest that OATP1B1 is a major transporter for rifampin (Tirona et al., 2003). Likewise, HMG-CoA) reductase inhibitors (statins) have also been shown to be highly dependent on OATP1B1 and OATP1B3 to exert their effects on intracellular hepatic HMG-CoA reductase and thereby reduce cardiovascular events associated with hypercholesterolemia and atherosclerosis (Schachter, 2005). Pravastatin has been widely studied as a substrate for OATP transporters including OATP1B1 and recent studies have linked single nucleotide polymorphisms (SNPs) in SLCO1B1 as a major predictor of pravastatin pharmacokinetics (Nakai et al., 2001; Ho et al., 2007).

We now provide data that suggest loss of Oatp1b2 (*Slco1b2*) does not result in a major phenotype in terms of viability or liver function, but the ability to eliminate drugs such as pravastatin and rifampin is significantly compromised. Taken together, our findings suggest that the *Slco1b2*(−/−) mouse model may prove to be a useful in vivo model for assessing the contribution of OATP1B transporters to the hepatic uptake of drugs.

Materials and Methods

Materials. Rifampin, diclofenac, dimethyl sulfoxide, and pravastatin were obtained from Sigma (St. Louis, MO). Atorvastatin was obtained from Pfizer Global Research and Development (Ann Arbor, MI). Ammonium formate and all other chemical reagents were obtained from Sigma. Isoflurane (IsoFlo) was obtained from Abbott Laboratories (Abbott Park, IL). All other compounds used were reagents grade.

Targeting of Slco1b2 in Mouse ES Cells. The targeting vector was designed using the *Slco1b2* genomic locus form the Celera mouse genomic sequence database and the mRNA sequence (NM_178235). As shown in Fig. 1, homologous recombination resulted in the deletion of a 6772-bp fragment containing exon 10 to 12 of the mouse *Slco1b2* genomic sequence and insertion of a neomycin resistance cassette. The 5′ and the 3′ regions of homology were amplified from DBA1/lacJ mouse genomic DNA using the Expand High Fidelity PCR system (Roche, Laval, QC, Canada). The primer pairs 5′-OAC-6141F, 5′-ggatccgagttgtcttttctgagtgttagg-3′; 5′-OAC-9873R, 5′-ggatccatgacagttgtctgctcattgc-3′; and 3′-OAC-17027F, 5′-ctcgagatgtttggctgagagcatctgc-3′; and 3′-OAC-21988R, 5′-gcggccgctcatcttcatagcaaccctttcc-3′ (F, forward; R, reverse) were used to amplify 4139- and 4962-bp fragments of the genomic DNA, respectively. The resulting PCR fragments were cloned into the pCR 2.1-TOPO vector (Invitrogen, Carlsbad, CA). After sequence verification, the homologous fragments were cloned into the backbone of the targeting vector plasmid that contained both a neomycin (neo) and a thymidine kinase expression cassette (see Fig. 1). Subsequently, the linearized *Slco1b2* targeting vector was electroporated into DBA1/lacJ ES cells. Those cells were cultured in the presence of G418 (positive selection attributable to neomycin cassette) and ganciclovir (negative selection attributable to thymidine kinase cassette) for selecting the correctly targeted ES cells.

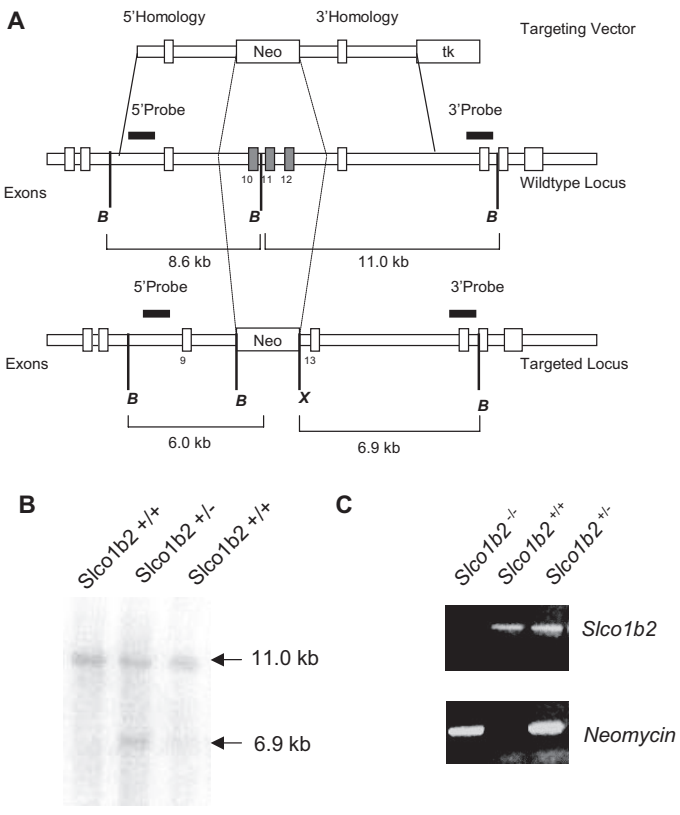

Fig. 1. The *Slco1b2* knockout mouse was generated by excision of exon 10 to 12 of the *Slco1b2* gene locus by standard targeting methods. The targeting vector consisted of 5′ and 3′ sequence homology arms flanking the neomycin selection (neo) cassette (A). For negative selection with ganciclovir, a thymidine kinase (tk) cassette was included in the targeting vector (A). Digest of the wild-type locus with BamHI resulted in a 11.0-kb fragment detected by Southern blotting using a 3′ probe for detection, whereas successful targeting with deletion of exon 10 to 12 resulted in a 6.9-kb fragment after digest with BamHI and XhoI (B). For genotyping of the resulting mice, PCRs detecting a fragment of the S*lco1b2* gene locus or neomycin were performed (C).

Southern Blot Screening of ES Cells for Slco1b2 Homologous Recombination. Southern Blot analysis was performed to screen for successful integration of the targeting vector that resulted in the deletion of exon 10 to exon 12 and insertion of the neomycin cassette. In brief, genomic DNA was isolated from ES cells after electroporation with the *Slco1b2* targeting vector and selection with G418/gancyclovir. DNA was digested with BamHI and XhoI. After electrophoretic separation on a 0.7% agarose gel (FMC BioProducts, Rockland, ME), the DNA was transferred to Hybond N+ nylon membrane (GE Healthcare, Chalfont St. Giles, Buckinghamshire, UK). For detection of the genomic DNA fragments, two probes were used to screen for homologous recombination between the *Slco1b2* targeting vector and endogenous locus. The 3′ Southern probe was a 717-bp fragment (OAC-23209F, 5′-cacttggaagcaaacattagtcc-3′ and OAC-23926R, 5′-taatccttgcaggaaagatacc-3′) that recognized an 11.0-kb endogenous *Slco1b2* BamHI fragment and also a 6.9-kb BamHI/XhoI fragment in a targeted clone. Clones demonstrating targeting with the 3′ probe were then confirmed by Southern analysis using a second probe spanning 524 bp of the endogenous locus (OAC-5660F, 5′-tatctgtcgctgtaccagtacc-3′; OAC-6184R, 5′-gatggttcactggagtactctgc-3′).

ES Cell Microinjection and Identification of Homozygote Slco1b2 Knockout Mice. *Slco1b2*-targeted ES cells (15–20 cells) were microinjected into blastocyst stage (3.5 days) C57BL/6 embryos (Charles River Laboratories, Wilmington, MA). Surviving embryos were implanted into the uteri of day 2.5 pseudopregnant CD-1 (Charles River Laboratories, Wilmington, MA) female mice. Chimeric male mice were identified from the offspring of these injections by the presence of mixed coat color, black (C57BL/6 host-derived) and brown (*Slco1b2* ES cell-derived). Chimeric male mice were bred with wild-type DBA1/LacJ female mice to identify *Slco1b2* ES cell-derived germline offspring. DNA was isolated from tail biopsies of the germline offspring and genotyped by PCR (neo-833F, 5′-gcaggatctcctgtcatctcacc-3′ and neo-1023R, 5′-gatgctcttcgtccagatcatcc-3′) for the presence (heterozygous, +/−) or absence (wild type, +/+) of the neomycin cassette. The neo-833F and neo-1023R oligonucleotide set amplifies a 190-bp fragment. *Slco1b2* heterozygous male and female mice were bred together to produce homozygous (−/−) knockouts. Offspring were genotyped by PCR using two oligonucleotide sets: the neo set and the other specific for part of the *Slco1b2* knockout region. The *Slco1b2* oligonucleotide set (OAC-15409F, 5′-tggacaatgtgcaatgggagc-3′; OAC-15906R, 5′-gaaagagctgattagagatacg-3′) amplifies a 497-bp fragment contained within the knockout region. Hence, by genotyping using these two oligonucleotide sets, a knockout (−/−) animal would be negative for the *Slco1b2* PCR and positive for the neo PCR. A heterozygous (+/−) mouse would be positive for both PCR sets. And a wild-type (+/+) mouse would be positive for the *Slco1b2* PCR but negative for the neo PCR.

Animals. Mice were housed in an American Association for Accreditation of Laboratory Animal Care International-accredited facility and handled according to Pfizer Global Research guidelines complying with the U.S. Public Health Service Policy for the Care and Use of Laboratory Animals. *Slco1b2* knockout and wild-type (DBA1/lacJ) mice were obtained from Pfizer Groton with breeding colony housing and expansion provided by Charles River Laboratories. All mice used in this report were between 9 and 14 weeks of age. Animals were kept in a temperature-controlled environment with a 12-h light/dark cycle and received a standard diet and water ad libitum.

Clinical Biochemistry. Serum separator tubes containing mouse blood collected at necropsy were allowed to stand at room temperature until clotted (approximately 30 min). Samples were then centrifuged for at least 8 min at <3500 rpm (2851 g) at 2–8°C to separate serum from the blood cells, minimizing changes in the electrolytes and preventing hemolysis of the samples. Samples were analyzed using the Advia 2400 Chemistry System (Bayer Corp., Diagnostics Div., Tarrytown, NY). Advia 2400 clinical chemistry assay methodology is based on the change in color from the reaction of the analyte in the sample fluid with method-specific reagents, and electrolytes are measured by a potentiometric procedure that uses ion-selective electrodes. Clinical laboratory data were collected using Cerner version 8, and treatment comparisons were performed by pair-wise comparison within one-factor analysis of variance.

Quantitative Real-Time PCR in Mouse Liver. Liver tissue was harvested from wild-type and *Slco1b2*(−/−) mice, snap frozen, and stored at −80°C until isolation of total RNA. After mechanical homogenization of the tissue, RNA was isolated and purified using the RNeasy Mini Kit (QIAGEN, Valencia, CA) according to the manufacturer's instructions. Subsequently, the amount and integrity of the isolated RNA was determined using an Agilent Bioanalyzer and the Agilent RNA 6000 Series II Nano Lab on Chip assay (Agilent, Santa Clara, CA). RNA was stored at −80°C.

Real-Time PCR. TaqMan Reverse Transcription Reagents supplied by Applied Biosystems (Foster City, CA) were used for reverse transcription of total RNA. Two micrograms of total RNA were transcribed in a 50-μl reaction containing 1× TaqMan RT buffer, 5.5 mM $MgCl_2$, 500 μM dNTPs, 2.5 μM random hexamers, 0.4 U/μl RNase inhibitor, and 1.25 U/μl Multiscribe Reverse Transcriptase. The reaction was performed under the following thermocycler conditions: 25°C for 10 min, 48°C for 30 min, and 95°C for 5 min. The resulting cDNA was used for quantitative real-time PCR.

Expression of *Slco1b2* (Oatp1b2), *Slco1a1* (Oatp1a1), *Slco1a4* (Oatp1a4), and 18S rRNA were determined using the TaqMan assays Mm00451513_m1, Mm00649796_m, Mm00453136_m1, and Hs99999901_s1, respectively, from Applied Biosystems. Expression of other transporters was determined using SYBR green assays. Primers are summarized in Table 1. For all assays, the recommended TaqMan cycler conditions were used.

Immunohistochemistry. Paraffin-embedded liver sections were deparaffinized in two changes of xylene (5 min each) followed by stepwise rehydration in decreasing ethanol and two washes in double-distilled H_2O. Heat-induced epitope retrieval was performed by boiling the slides in citrate buffer, pH 6.0. After several rinses in

TABLE 1
Primers used for quantification of hepatic transporter expression in mice

Gene	Primer Sequences	Reference
Abcc2		
Forward	5′-CTGAGTGCTTGGACCAGTGA-3′	
Reverse	5′-CAAAGTCTGGGGGAGTGTGT-3′	
Abcc3		
Forward	5′-CGCTCTCAGCTCACCATCAT-3′	
Reverse	5′-GGTCATCCGTCTCCAAGTCA-3′	
Abcc4		
Forward	5′-TTAGATGGCCTCTGGTTCT-3′	Wagner et al., 2003
Reverse	5′-GCCCACAATTCCAACCTTT-3′	
Abcg2		
Forward	5′-AATGGAGCACCTCAACCTG-3′	Han and Sugiyama, 2006
Reverse	5′-CCCATCACAACGTCATCTTG-3′	
Ostα		
Forward	5′-GTCTCAAGTGATGAACTGCCA-3′	Zollner et al., 2006
Reverse	5′-TTGAGTGCTGAGTCCAGGTC-3′	
Ostβ		
Forward	5′-GTATTTTCGTGCAGAAGATGCG-3′	Zollner et al., 2006
Reverse	5′-TTTCTGTTTGCCAGGATGCTC-3′	
Abcb11		
Forward	5′-GTTCAGTTCCTCCGTTCAAA-3′	
Reverse	5′-AAGCTGCACTGTCTTTTCAC-3′	
Slc10a1		
Forward	5′-CACCATGGAGTTCAGCAAGA-3′	Wagner et al., 2005
Reverse	5′-AGCACTGAGGGGCATGATAC-3′	
Abcb1b		
Forward	5′-TGCTTATGGATCCCAGAGTGAC-3′	
Reverse	5′-TTGGTGAGGATCTCTCCGGCT-3′	
Slc22a7		
Forward	5′-CAGCTCCGACACGTCTCACT-3′	
Reverse	5′-TGTCTGGTACACGGTCAGCC-3′	

ice-cold PBS, the sections were incubated with 5% fetal bovine serum (FBS) diluted in phosphate-buffered saline (PBS) for 1.5 h, followed by an overnight incubation at 4°C with the primary antibody diluted 1:50 in 5% FBS-PBS. The primary antibody against oatp1b2 is a novel custom antibody raised in rabbits immunized against the following epitope specific for murine oatp1b2: KNPVTNPTTQEKQA-PAN (Invitrogen). After several washes in PBS, the slides were incubated with the secondary anti-rabbit antibody provided in the Vectastain Kit (Vector Laboratories, Burlington, ON, Canada), which was then visualized using 3-amino-9-ethylcarbazole substrate provided by Vector Laboratories.

Crude Membrane Preparation from Mouse Liver Tissue. Mouse liver tissue was homogenized in 5 mM Tris-HCl, pH 7.5, containing protease inhibitors (Sigma Aldrich) using a Potter Elvehjem homogenizer. After 2 × 20 strokes on ice, the homogenate was incubated on ice under continuous stirring. Subsequently, the homogenate was centrifuged at 9000*g* for 20 min at 4°C. The supernatant was transferred to an ultracentrifuge tube and centrifuged for 45 min at 100,000*g* at 4°C. The resulting pellet was dissolved in 5 mM Tris-HCl supplemented with protease inhibitors. Protein content was determined by BCA method (Pierce, Rockford, IL).

Western Blot Analysis. After separating the crude membrane fraction by SDS-polyacrylamide gel electrophoresis using 4 to 12% gradient acrylamide gels (NuPAGE, Invitrogen), the separated proteins were electrotransferred to a nitrocellulose membrane using a tank blotting system. The transfer of protein was assessed by Ponceau S staining (Sigma-Aldrich). Subsequently, the membranes were incubated in 5% low fat milk powder in TBS-T (Tris-buffered saline and 0.1% Tween 20) for 2 h. Afterward, the membrane was incubated with the anti-mouse Oatp1b2 antibody at a dilution of 1:2000 or anti-calnexin at a dilution of 1:4000. After overnight incubation at 4°C, several washing steps with TBS-T and an additional incubation for 1.5 h with 5% FBS in TBS-T, the blot was incubated with a horseradish peroxidase-labeled anti-rabbit secondary antibody (Bio-Rad Laboratories, Hercules, CA) diluted 1:2000 for 2 h. Before visualizing the immobilized secondary antibody using ECL Plus Reagent (GE Healthcare), the blot was washed in several changes of TBS-T. The chemiluminescent signal was detected using the KODAK ImageStation 4000MM (Mandel, Guelph, ON, Canada).

Rifampin and Pravastatin Pharmacokinetics in Slco1b2(−/−) and Wild-Type Mice. Male *Slco1b2* knockout and wild-type mice were obtained from Pfizer Groton (bred in-house by Genetic Technology). Mice received an intravenous dose of rifampin (1 mg/kg in 0.5% dimethyl sulfoxide in water) through the tail vein. At predetermined time points, mice were anesthetized with isoflurane, and blood samples were obtained by cardiac puncture and transferred to EDTA-containing tubes. Plasma was retrieved after centrifugation of blood. Liver tissues were also collected from animals and all samples were stored at −80°C until analyzed by liquid chromatography/tandem mass spectrometry (LC-MS/MS).

Rifampin and Pravastatin Continuous Subcutaneous Infusion in Slco1b2(−/−). Alzet mini-osmotic pumps (model 201D) were purchased from Durect Corporation (Cupertino, CA). Male wild-type and *Slco1b2* knockout mice (n = 4/genotype) had the mini pump containing dosing solution implanted dorsally (rate of drug release, 8 μl/h). For rifampin determination, blood samples were collected by cardiac puncture 24 h after pump insertion, samples were centrifuged (3000*g*) to obtain plasma, and livers were collected for storage at −80°C until analyzed by LC-MS/MS. For pravastatin analysis, blood samples were obtained by cardiac puncture and transferred to tubes containing 0.72 mg of NaF and 0.58 mg of potassium oxalate. Plasma was obtained by centrifugation. Subsequently, 10% 6 M ammonium acetate, pH 4.5, was added to all pravastatin plasma samples. Liver tissues were reconstituted and homogenized in 6 M ammonium acetate, pH 4.5. All samples were stored at −80°C until analyzed by LC-MS/MS.

Quantitation of Pravastatin and Rifampin Levels. LC-MS/MS analysis was carried out using a high-performance liquid chromatography system consisting of a LC-10AD pump (Shimadzu Europe, Duisberg, Germany) with CTC PAL autosampler (Leap Technologies, Carrboro, NC) interfaced to a TSQ Quantum Ultra mass spectrometer (Thermo Fisher Scientific, Waltham, MA). Rifampin and internal standard (diclofenac) were separated on an Atlantis dc18 5-μm column (2.1 × 50 mm). The mobile phase consisted of solvent A (5 mM ammonium formate with 0.1% formic acid) and solvent B (acetonitrile). The gradient was as follows: solvent B was held at 10% for 0.3 min, ramped from 10% to 90% over 1.7 min, ramped from 90% to 95% over 0.8 min, and then immediately brought back down to 10% for re-equilibration. Total run time was 3.5 min with a flow rate of 0.30 ml/min. The mass spectrometer was operated in positive ion electrospray ionization for the detection of rifampin and diclofenac. Multiple reaction monitoring analysis was performed with the following transitions: m/z 823 → 791 (rifampin) and m/z 296 → 215 (diclofenac). Standard samples in the appropriate drug-free matrix were prepared, yielding a concentration range from 9.75 to 10,000 ng/ml. Pravastatin and the internal standard (atorvastatin) were separated on a Hypersil Gold column (2.1 × 50 mm; Thermo Fisher Scientific) by gradient elution. The mobile phase consisted of solvent A (5 mM ammonium formate in water) and solvent B (acetonitrile). The gradient was as follows: solvent B was held at 25% for 0.3 min, linearly ramped from 25 to 95% over 1.8 min, held at 95% for 0.7 min. and then immediately brought back to 25% for re-equilibration. Total run time was 3 min with a flow rate of 0.275 ml/min. The mass spectrometer was operated in negative ion electrospray ionization mode for the detection of pravastatin and atorvastatin. Multiple reaction monitoring was performed with the transitions m/z 423 → 101 for pravastatin and m/z 557 → 278 for atorvastatin. All raw data were processed using Analyst Software (ver. 1.4.1; Applied Biosystems/MDS Sciex Inc., Mississauga, ON, Canada). Calibration standards were prepared from the high calibration standard by serial dilution to the following levels: 1000, 500, 125, 31.5, and 3.9 ng/ml in mouse plasma. Pravastatin standard curve samples were prepared in appropriate drug-free matrix, yielding a concentration range from 3.9 to 2000 ng/ml.

Pharmacokinetic Calculations and Statistical Analysis. Rifampin clearance (CL) after IV bolus was calculated as dose/AUC, where AUC is the area under the plasma concentration-time profile from t = 0 to ∞. Volume of distribution at steady state (V_{SS}) was calculated as (AUMC × dose)/AUC^2, where AUMC is the area under the moment curve. The Student's t test was used to evaluate statistical significance between *Slco1b2*(−/−) and wild-type mice in gene expression and in pharmacokinetic studies.

Results

Targeted Deletion and Characterization of Slco1b2(−/−) Mice. The *Slco1b2*(−/−) mice were generated by deleting a 6772-bp fragment spanning exons 10 to 12 in the genomic DNA locus (Fig. 1A) with replacement with a neomycin resistance gene cassette through homologous recombination in mouse embryonic stem cells derived from DBA1/LacJ mice. DNA obtained from ES cells resistant to neomycin and ganciclovir was used for Southern blot analysis using two different probes detecting a 6.9-kb fragment compared with 11.0-kb fragments present in wild-type DNA (Fig. 1B). Two targeted ES cell clones were identified from 189 clones screened. Karyotype analysis was done on these clones and both were shown to have normal 40XY karyotypes. Genotyping was carried out performing PCRs specific for *Slco1b2* and neomycin identifying homozygote and heterozygote offspring (Fig. 1C). Mice homozygous for the disrupted allele, designated *Slco1b2*(−/−), were born normally and appeared indistinguishable from their wild-type counterparts. No differences were found between litter size and

growth rates for the *Slco1b2*(−/−) animals compared with wild-type littermate controls. The resulting *Slco1b2*(−/−) mice displayed no obvious phenotype, and livers appear macroscopically and histologically normal.

Comparison of oatp1b2 Expression in Wild-Type and *Slco1b2*(−/−) Mice. We used a novel custom synthesized anti-mouse Oatp1b2-antibody to conduct Western blot analysis and noted the lack of Oatp1b2 protein (~65 kDa) in the liver homogenate of *Slco1b2*(−/−) mice (Fig. 2A). Immunohistochemical staining of paraffin sections using the same antibody demonstrated clear expression of Oatp1b2 on the basal membrane facing the perisinusoidal space of hepatocytes in the wild-type but not in *Slco1b2*(−/−) mice (Fig. 2, B and C). Moreover, quantitative real-time PCR analysis revealed that Slco1b2 mRNA expression was markedly lower in the *Slco1b2*(−/−) livers relative to the wild-type mice livers, suggesting that transcript lacking the deleted exons are unstable or rapidly degraded. Note that detection of low-level *Slco1b2* transcript in the *Slco1b2* knockout mice is not unexpected because the primers and probe used for detection encompass exons 3 and 4. It is noteworthy that wild-type female mice seemed to express higher mRNA levels of the transporter compared with wild-type male mice (mean relative expression of *Slco1b2* ± S.D.: wild-type female, 1.47 ± 0.33; wild-type male, 1.01 ± 0.16; $p < 0.05$).

Serum Biochemical Analysis. Serum biochemical analysis revealed no significant changes in markers of liver function such as alanine aminotransferase or aspartate aminotransferase. Moreover, no changes were observed in the serum levels of triglycerides, chloride, sodium, potassium, creatinine, or urea nitrogen. However, a modest elevation of total bilirubin levels was detected in *Slco1b2*(−/−) mice (table 2). Further analysis revealed that most of the plasma bilirubin was conjugated to suggest Oatp1b2 may be involved in hepatic reuptake of conjugated bilirubin from circulation.

Expression of Other Hepatic Oatp Transporters. To determine whether compensatory changes in expression of other hepatic Oatp transporters occurred in the *Slco1b2*(−/−) mice, real-time PCR was performed to quantitate expression of *Slco1a1*, (*Oatp1a1*, *Oatp1*), *Slco1a4* (*Oatp1a4*, *Oatp2*), and *Slco2b1* (*Oatp2b1*, *Oatp-b*). Slco1al mRNA did not differ between wild-type and *Slco1b2*(−/−) animals [Fig. 3, top; mean *Slco1a1* expression relative to wild-type male ± S.D.: female wild-type, 0.64 ± 0.26; female *Slco1b2*(−/−), 0.68 ± 0.1; male wild-type, 1.02 ± 0.22; male *Slco1b2*(−/−), 1.22 ± 0.32; $n = 5$]. However, *Slco1a4* [Fig. 3B; mean relative *Slco1a4* expression ± S.D.: female wild-type, 5.198 ± 1.417, female *Slco1b2*(−/−), 11.31 ± 5.24; $p < 0.05$, $n = 5$] and oatp2b1 [Fig. 3C; mean relative *Slco2b1* expression ± S.D.: female wild-type, 1.97 ± 0.5; female *Slco1b2*(−/−), 3.21 ± 1.30; $p <$

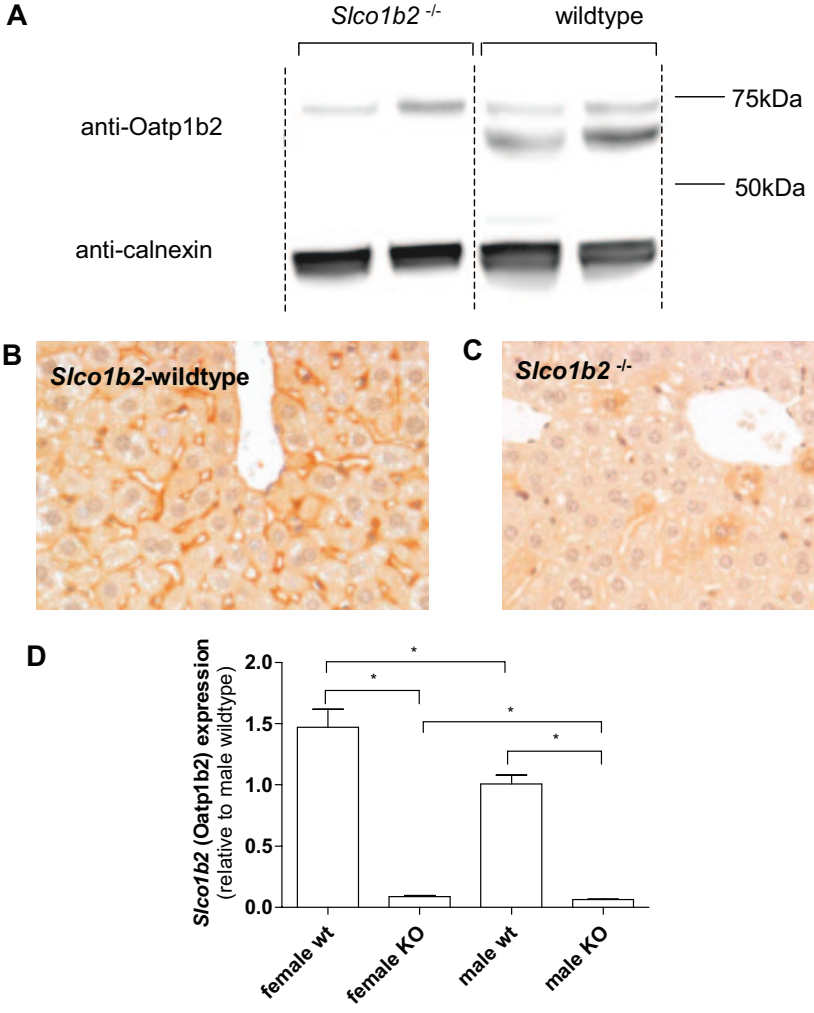

Fig. 2. Detection of Oatp1b2 by Western blot analysis revealed the absence of Oatp1b2 expression in *Slco1b2*(−/−) mice (A). Immunohistochemical staining of Oatp1b2 (red) in mouse liver showed expression of the transporter in the basal membrane of hepatocytes (B). In animals with targeted disruption of *Slco1b2*, expression of the transporter was not detectible (C). mRNA expression was assessed by real-time RT-PCR and showed a significant reduction of *Slco1b2* in knockout animals (D).

TABLE 2
Serum biochemistry comparing wild-type and *Slco1b2*(−/−) animals.

Parameter	Wild-Type	*Slco1b2*(−/−)
Triglycerides (mg/dl)	119.00 ± 7.02	110.67 ± 9.87
Aspartate aminotransferase (U/l)	129.00 ± 78.72	123.00 ± 38.66
Alanine aminotransferase (U/l)	42.75 ± 5.62	66.5 ± 29.38
Total bilirubin (mg/dl)	0.10 ± 0.00	0.23 ± 0.05*
Chloride (mM)	111.75 ± 1.71	112.00 ± 2.16
Sodium (mM)	149.00 ± 0.00	148.75 ± 0.96
Potassium (mM)	5.50 ± 0.18	5.28 ± 0.22
Creatinine (mg/dl)	0.2 ± 0.0	0.2 ± 0.0
Urea nitrogen (mg/dl)	21.50 ± 1.73	20.25 ± 0.50

* $p < 0.05$

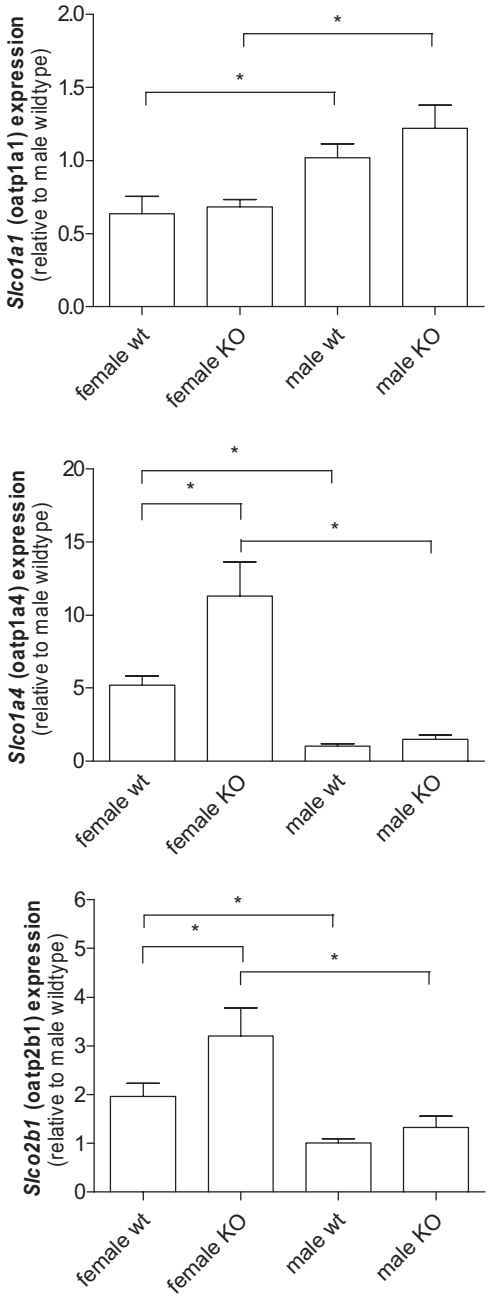

Fig. 3. Hepatic mRNA expression of *Slco1a1* (Oatp1a1), *Slco1a4* (Oatp1a4), and *Slco2b1* (Oatp2b1) as determined by real-time PCR comparing wild-type and *Slco1b2*(−/−) animals. *, $p < 0.05$.

0.05, $n = 5$] levels were significantly greater only in the female *Slco1b2*(−/−). No differences in hepatic *Slco1a4* expression were detected in male wild-type versus *Slco1b2*(−/−) mice [Fig. 3, center; mean relative *Slco1a4* expression ± S.D.: male wild-type, 1.04 ± 0.32; male *Slco1b2*(−/−) male, 1.49 ± 0.58, $n = 5$]. Again, no difference in expression was noted for *Slco2b1* expression in male wild-type versus *Slco1b2*(−/−) mice [Fig. 3, bottom; mean relative *Slco2b1* expression ± S.D.: male wild-type, 1.01 ± 0.19; male *Slco1b2*(−/−), 1.33 ± 0.47, $n = 5$]. Expression of other hepatic transporters was measured, including efflux transporters *Abcc2*, *Abcc3*, *Abcc4*, *Abcg2*, *Abcb1b*, and *Abcb11* and the uptake transporters *Slc10a1*, *Ostα*, *Ostβ*, and *Slc22a7*. Although modest gender-dependent differences were noted to be statistically different for *Abbc4*, *Ostβ*, and *Slc22a7*, for the most part, no major differences were noted in the basal expressed levels of other uptake and efflux transporters (Table 3).

Rifampin Pharmacokinetics and Liver/Plasma Ratio in Slco1b2(−/−) and Wild-Type Mice. To assess the in vivo relevance of Oatp1b2, rifampin disposition was compared between male *Slco1b2*(−/−) and wild-type animals. First, we examined rifampin pharmacokinetics after a single intravenous dose of 1 mg/kg. As shown in Fig. 4, A and B, there were significantly higher plasma rifampin levels in mice lacking Oatp1b2 expression. The plasma AUC in knockout mice was 1.7-fold greater than in wild-type mice [mean rifampin plasma AUC ± S.D.: wild-type animals, 19,586 ± 5971 ng·hr/ml; *Slco1b2*(−/−) animals, 31,931 ± 4949 ng·hr/ml; $p < 0.05$]. However, and consistent with Oatp1b2 function as a hepatic rifampin uptake transporter, mice lacking Oatp1b2 had a 2.5-fold reduction in liver rifampin exposure [mean rifampin AUC ± S.D.: wild-type animals, 206,434 ± 140,712 ng·hr/g; *Slco1b2*(−/−) animals, 86,781 ± 58,433 ng·hr/g; $p = 0.055$]. Liver-to-plasma concentration ratios were also determined for both genotypes and revealed a significant difference between wild-type and *Slco1b2*(−/−) animals (Table 4). The plasma clearance of rifampin in *Slco1b2*(−/−) mice was 43% lower than wild-type mice [mean plasma clearance ± S.D.: wild-type mice, 56 ± 20 ml/h/kg; *Slco1b2*(−/−) mice, 32 ± 5 ml/h/kg; $p < 0.05$] indicating that reduced uptake into liver had marked effects on drug elimination. Furthermore, the rifampin V_{SS} in *Slco1b2*(−/−) mice was 67% smaller than in wild-type mice (mean V_{SS} ± S.D.: wild-type mice, 374 ± 244 ml/kg; *Slco1b2*(−/−) mice, 124 ±

TABLE 3
Expression of hepatic drug transporters in mouse liver comparing wild-type and *Slco1b2*-knockout animals.
Data are presented as mean expression relative to wild-type male animals ± S.D.

	Wild-Type		*Slco1b2*(−/−)	
	Female	Male	Female	Male
Abcc2	1.36 ± 0.56	1.01 ± 0.14	1.71 ± 0.58	0.90 ± 0.45
Abcc3	1.99 ± 0.60	1.08 ± 0.36	2.83 ± 1.19	1.53 ± 0.35
Abcc4	1.67 ± 0.29	1.03 ± 0.25	3.03 ± 0.47*	1.51 ± 0.63
Abcg2	0.32 ± 0.06	1.01 ± 0.15	0.47 ± 0.14	1.11 ± 0.22
Ostα	1.05 ± 0.42	1.10 ± 0.47	1.94 ± 3.47	2.89 ± 3.47
Ostβ	3.65 ± 1.04	1.03 ± 0.29	3.61 ± 2.24	0.62 ± 0.18*
Abcb11	0.71 ± 0.19	1.05 ± 0.33	0.98 ± 0.18*	0.79 ± 0.37
Slc10a1	3.04 ± 1.51	1.20 ± 0.62	4.18 ± 3.93	1.87 ± 2.00
Abcb1b	0.41 ± 0.09	1.03 ± 0.26	0.75 ± 0.35	1.94 ± 0.35
Slc22a7	1.76 ± 0.71	1.01 ± 0.12	1.16 ± 0.42*	0.75 ± 0.08

* $p < 0.05$

18 ml/kg; $p = 0.054$), suggesting that the liver is a major organ for rifampin distribution and that Oatp1b2 plays a significant role.

To further understand the role of Oatp1b2 activity with respect to rifampin clearance, we carried out additional studies of rifampin concentrations in plasma and liver tissues at steady-state conditions. After 24 h of continuous subcutaneous infusion of rifampin at a rate of 8 μg/h, the measured liver concentration of rifampin was significantly decreased in *Slco1b2*(−/−) animals [mean liver concentration ± S.D.: wild-type animals, 9440 ± 1904 ng/g; *Slco1b2*(−/−) animals, 2348 ± 196 ng/g; $p < 0.05$] (Fig. 4C). This result was coupled with significantly higher steady-state plasma concentrations in knockout mice [mean rifampin steady-state plasma concentration ± S.D.: wild-type animals, 249 ± 70 ng/ml; *Slco1b2*(−/−) animals, 480 ± 113 ng/g; $p < 0.05$] (Fig. 4D). Our data strongly suggest that Oatp1b2 is a major contributor of hepatic rifampin uptake and clearly shows the relevance of this transporter in altering liver-to-plasma ratio of this drug (mean plasma-to-liver ratio ± S.D.: wild-type animals, 39.0 ± 6.5; *Slco1b2*(−/−) animals, 5.2 ± 2.1; $p < 0.05$) (Fig. 4E).

Pravastatin Pharmacokinetics and Liver/Plasma Ratio in Slco1b2(−/−) and Wild-Type Mice. Given the widely accepted notion that pravastatin is an excellent probe substrate of OATP transporters, we extended our investigations to assess the disposition profile of this drug. The male mice were given constant infusion of low-dose-rate (8 μg/h) and high-dose-rate (32 μg/h) pravastatin. As shown in Fig. 5A, when administered the low-dose-rate subcutaneous infusion, steady-state plasma concentrations of pravastatin were 1.8-fold higher in knockout compared with wild-type mice (12 ± 2.2 versus 6.5 ± 1.3 ng/ml; $p < 0.05$). Conversely, hepatic concentrations were 1.8-fold higher in wild-type compared with knockout mice (172 ± 17 versus 95 ± 6 ng/g; $p < 0.05$) (Fig. 5B), resulting in significant differences in the plasma-to-liver ratio of pravastatin [liver-to-plasma ratio ± S.D.: wild-type animals, 26.9 ± 3.4; *Slco1b2*(−/−) animals, 8.6 ± 1.0; $p < 0.05$; Fig. 5C]. Similar results were obtained after treating the animals with the high-rate infusion. As shown in Fig. 5, D–F, knockout animals consistently exhibited elevated pravastatin plasma levels [mean plasma level ± S.D.: wild-type, 114.7 ± 14.0 ng/ml; *Slco1b2*(−/−), 209.9 ± 14.2 ng/ml; $p < 0.05$] and correspondingly lower liver concentrations in the *Slco1b2*(−/−) knockout mice [mean liver level ± S.D.: wild-type, 647.0 ± 282.7 ng/g; *Slco1b2*(−/−), 343.8 ± 70.8 ng/g; $p = 0.053$].

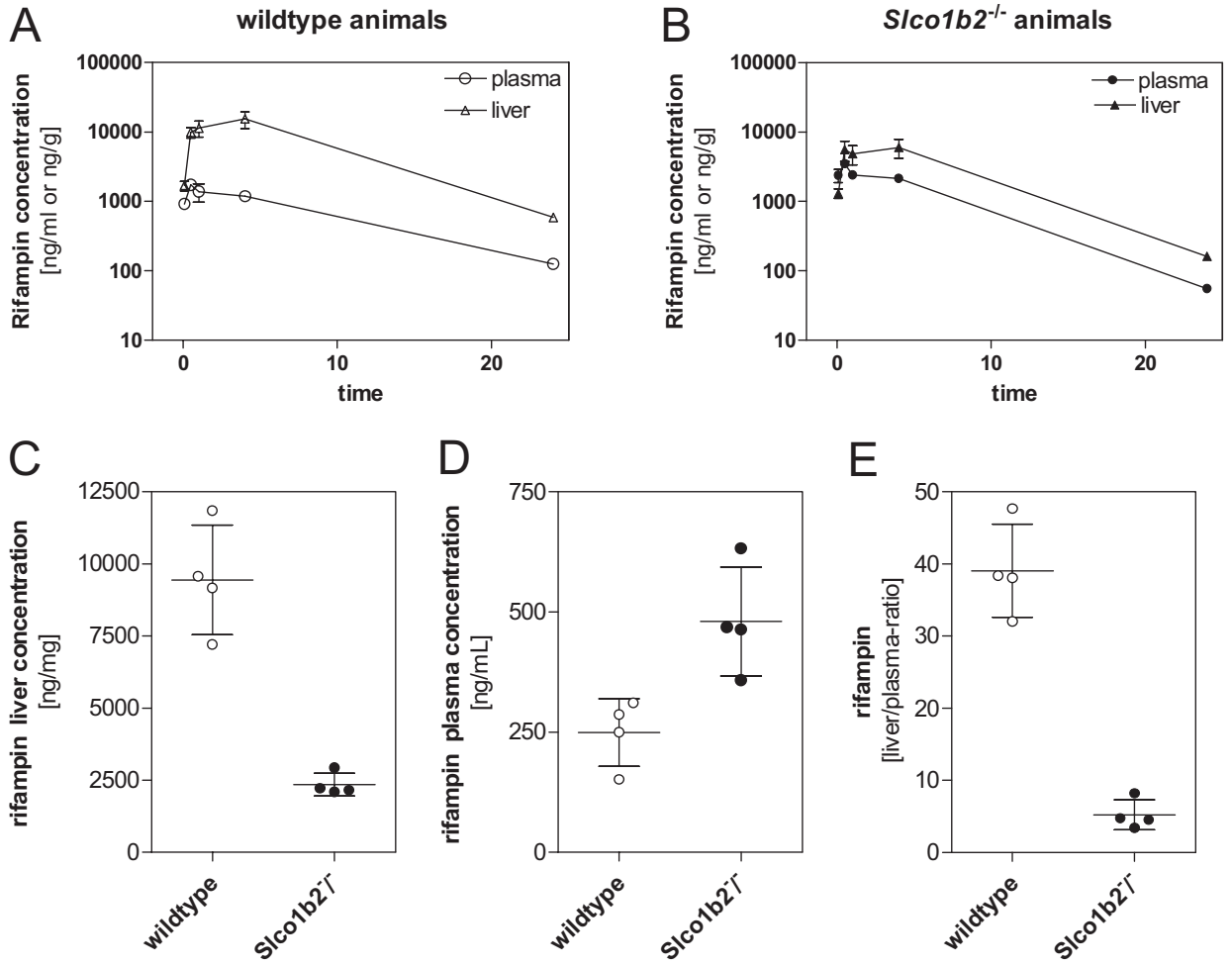

Fig. 4. Rifampin concentration in plasma (○) and liver (△) of wild-type (△) and *Slco1b2*(−/−) (B) mice ($n = 5$–6/time point) after a single intravenous dose of rifampin (1 mg/kg). Steady-state rifampin concentration in liver (C) and plasma (D) in animals treated with continuous subcutaneous infusion of rifampin at a rate of 8 μg/h over 24 h using Alzet Miniosmotic pumps (Durect Corporation) ($n = 4$). E shows the calculated liver-to-plasma ratio comparing wild-type and *Slco1b2*(−/−) animals. Data are expressed as mean ± S.D.

Discussion

In the past decade, molecular cloning and functional characterization of drug transporters have significantly changed our view of the mechanisms underlying drug absorption, distribution, and elimination. It is clear that in every tissue compartment, expression of an array of transporters that mediate the cellular uptake and efflux of endo- and xenobiotics is required to maintain target tissue or organ homeostasis. Indeed, in organs that are critical to the drug disposition process, such as liver and intestine, the predominant expression of certain types or classes of transporters with broad substrate specificity facilitates the intestinal absorption and efficient hepatic extraction of drugs for subsequent metabolism and biliary elimination.

The clinical relevance of a number of efflux transporters such as MDR1 (P-glycoprotein) and various MRP (ATP-binding cassette transporter) transporters has been clarified via the creation and study of efflux transporter gene knockout mouse models. However, for uptake transporters, only recently have there been the reports of such models (Jonker et al., 2001; Sweet et al., 2002; Eraly et al., 2006). In terms of hepatic drug uptake transporters, members of the OATP superfamily are believed to be the major determinants governing the hepatic extraction, drug-drug interactions, and in some cases, drug/toxin-induced liver injury. However, a mouse Oatp knockout model has yet to be reported. Among the OATP transporters expressed in human liver, OATP1B subfamily members OATP1B1 and OATP1B3 have been shown to be by far the most relevant to drug disposition because of their broad substrate specificity, expressed levels, and available genotype-to-phenotype correlations (Tirona and Kim, 2007). Therefore in addition to in vitro models for studying the activity of individual transporters, creation and pharmacological assessment of a murine *Slco1b2* knockout model has the potential to be a valuable preclinical model for delineating the in vivo role and relative contribution of hepatic OATP1B transporters to drug substrates identified using in vitro systems.

Our data strongly support a major role for Oatp1b2 in the hepatic uptake of drugs as shown by 3- to 8-fold lower liver-to-plasma ratio of prototypical substrate drugs pravastatin and rifampin in knockout compared with wild-type mice (Figs. 4C and 5C).

We also note that there does not seem to be a major compensatory up-regulation of other Oatps expressed in rodent liver, such as Oatp1a1, Oatp1a4, and Oatp2b1, although gender-related differences were noted (Fig. 3, A–C). This suggest that Oatp1b2, in addition to transporting xenobiotic substrates, may transport hormone or hormone metabolites that are essential in female mice. Expression of other hepatic

TABLE 4

Liver-to-plasma ratio comparing wild-type and *Slco1b2*(−/−) animals after a single intravenous dose of rifampin (1 mg/kg)

Data are expressed as mean liver-to-plasma ratio (mean ± S.D.).

Time	Wild-Type	*Slco1b2*(−/−)
5 min	2.0 ± 1.2	0.6 ± 0.3*
15 min	5.8 ± 2.9	1.6 ± 1.0*
30 min	11.9 ± 6.7	2.4 ± 2.4*
1 h	18.0 ± 16.6	3.0 ± 2.2
4 h	4.7 ± 1.3	3.0 ± 0.4*

* $P < 0.05$.

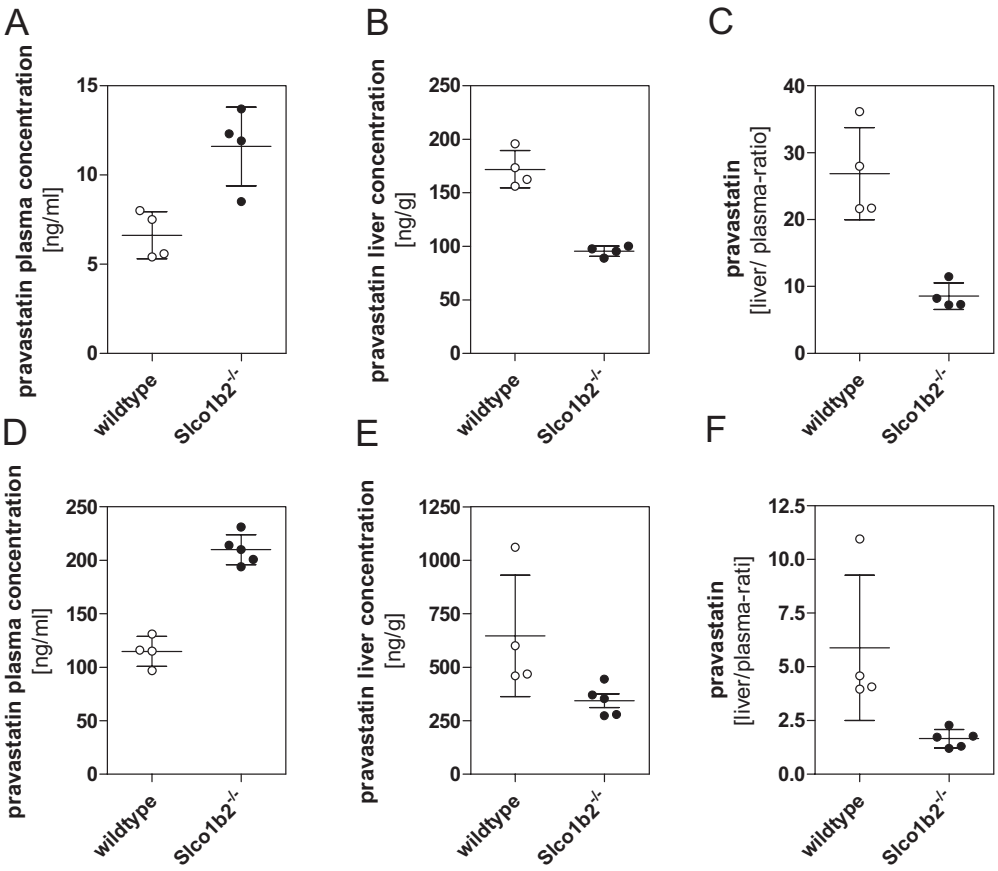

Fig. 5. Steady-state concentrations of pravastatin comparing wild-type (○) and *Slco1b2*(−/−) (●) animals. The concentration of pravastatin was determined in plasma (A and D) and liver (B and E) after 24-h subcutaneous infusion of low-dose-rate (8 μg/h) ($n = 4$) or high-dose-rate (32 μg/h) ($n = 5$) pravastatin using Alzet Miniosmotic pumps. The liver-to-plasma ratios are shown in C and F.

transporters for the most part was not affected (Table 3). Although the mice exhibited a mild elevation in basal total bilirubin level, we observed no jaundice at any stage postpartum to suggest Oatp1b2 is essential for hepatic bilirubin clearance. Moreover, most of the measured bilirubin seemed to be conjugated bilirubin, suggesting that the mild elevation in bilirubin may be due to loss of Oatp1b2-mediated hepatic reuptake of conjugated bilirubin (Table 2). Therefore, it seems likely other transporters expressed in liver are capable of efficient unconjugated bilirubin removal and Oatp1b2 alone does not seem to significantly alter unconjugated bilirubin clearance. Taken together, our findings of normal liver function, histology, and lack of any other overt phenotype, Oatp1b2, and likely human OATP1B1 and 1B3 play a clinically relevant function in terms of xenobiotic response and clearance.

It is also important to recognize that extensive studies of Oatp1a1 and Oatp1a4 have suggested both of these transporters to be also highly expressed in liver and to possess broad substrate specificity. In fact, it has been shown that rat Oatp1a1 is capable of transporting pravastatin (Hsiang et al., 1999), and rifampin interacts with rat Oatp1a4 (*Slco1a4*) (Vavricka et al., 2002). Yet in our *Slco1b2*(−/−) mice, profound differences in the liver-to-plasma ratios for both drugs were noted (Fig. 4 and 5). Pravastatin liver-to-plasma ratio during infusion is greater during low infusion rate compared with high infusion rate (Fig. 5, C and F), probably because of saturation of uptake transport. For rifampin, our data show time-dependent changes in the liver-to-plasma rifampin concentration ratio after intravenous bolus. Initial liver-to-plasma ratios up to 1 h are more reflective of hepatic uptake processes than elimination or efflux. After 4 h, distribution equilibrium was observed, as is evidenced by approximate parallel declines in log plasma and liver rifampin concentrations over time. Indeed, liver-to-plasma ratios are up to 6-fold higher in *Slco1b2*(−/−) mice than wild-type mice during the initial distribution phase, indicating that hepatic rifampin uptake is impaired. During infusion of rifampin at steady-state, the liver-to-plasma ratio of rifampin is approximately 8-fold greater in *Slco1b2*(−/−) mice than wild-type mice. At this steady-state, hepatic drug levels will be controlled by the interplay of uptake, metabolism, and efflux processes. Because the liver-to-plasma ratio differences between knockout and wild-type mice at steady state are close in magnitude to that during the initial distribution phase after IV bolus, this again suggests that Oatp1b2-mediated uptake plays a rate-limiting role in hepatic rifampin clearance.

Overall, our current findings would support the notion that members of the OATP1B subfamily are major contributors to hepatocellular uptake and therefore efficacy of most HMG-CoA reductase inhibitors in clinical use today. Accordingly, reliance on only in vitro studies to identify drug substrates of Oatp transporters are likely to prove detrimental or inadequate in terms of being able to accurately predict which of them significantly affect drug disposition in vivo.

Note that although we recognize that a large list of drug substrates for Oatp/OATP transporters currently exists (Tirona and Kim, 2007), the key focus of this study was to use prototypical substrates of human OATP1B1 and -1B3 to determine whether an alteration in the disposition of such compounds are observed in the mouse model of Oatp1b2 deficiency. As noted earlier, our findings would support the utility of this mouse model for predicting the in vivo contribution of human OATP1B1 and -1B3. Note that in rodent liver, although Oatp1a1 and Oatp1a4 are highly expressed, direct human orthologs of such Oatps do not exist, and human OATP1A2 is not found in hepatocytes. Therefore, deducting the role of Oatp1a1 and Oatp1a4 may prove to be difficult when the liver-to-plasma ratio of OATP1B1 and -1B3 substrate drugs do not change in the *Slco1b2*(−/−) mice. It is likely that additional murine *Slco* genes will need to be deleted and relevant human *SLCO* genes introduced to more fully replicate human hepatic drug uptake capabilities. Nevertheless, as shown by our data using pravastatin and rifampin, important new insights to the in vivo relevance of Oatp1b2 can already be obtained through a systematic evaluation of the pharmacological response using this novel Oatp transporter knockout model.

In conclusion, to our knowledge, this is a first report to describe and detail a functional characterization of a murine Oatp transporter knockout model. We focused on Oatp1b2 because, in humans, members of the OATP1B subfamily have turned out to be key determinants governing the hepatic uptake of many drugs in clinical use, including the statin class of lipid-lowering drugs. Accordingly, data presented in this study show the utility of the *Slco1b2*(−/−) mouse model in terms of in vivo pharmacological and functional assessment of hepatic OATP1B-mediated hepatic drug uptake and may therefore be a useful tool for understanding the contribution of hepatic uptake transporters in drug disposition.

Acknowledgments

We thank Dr. Ute I. Schwarz (Division of Clinical Pharmacology, University of Western Ontario) for helpful discussions.

References

Abe T, Kakyo M, Tokui T, Nakagomi R, Nishio T, Nakai D, Nomura H, Unno M, Suzuki M, Naitoh T, Matsuno S, and Yawo H (1999) Identification of a novel gene family encoding human liver-specific organic anion transporter LST-1. *J Biol Chem* **274:**17159–17163.

Abe T, Unno M, Onogawa T, Tokui T, Kondo TN, Nakagomi R, Adachi H, Fujiwara K, Okabe M, Suzuki T, et al. (2001) LST-2, a human liver-specific organic anion transporter, determines methotrexate sensitivity in gastrointestinal cancers. *Gastroenterology* **120:**1689–1699.

Cattori V, Hagenbuch B, Hagenbuch N, Stieger B, Ha R, Winterhalter KE, and Meier PJ (2000) Identification of organic anion transporting polypeptide 4 (Oatp4) as a major full-length isoform of the liver-specific transporter-1 (rlst-1) in rat liver. *FEBS Lett* **474:**242–245.

Choudhuri S, Ogura K, and Klaassen CD (2000) Cloning of the full-length coding sequence of rat liver-specific organic anion transporter-1 (rlst-1) and a splice variant and partial characterization of the rat lst-1 gene. *Biochem Biophys Res Commun* **274:**79–86.

Eraly SA, Vallon V, Vaughn DA, Gangoiti JA, Richter K, Nagle M, Monte JC, Rieg T, Truong DM, Long JM, et al. (2006) Decreased renal organic anion secretion and plasma accumulation of endogenous organic anions in OAT1 knock-out mice. *J Biol Chem* **281:**5072–5083.

Hagenbuch B and Meier PJ (2004) Organic anion transporting polypeptides of the OATP/SLC21 family: phylogenetic classification as OATP/SLCO superfamily, new nomenclature and molecular/functional properties. *Pflugers Arch* **447:**653–665.

Han Y and Sugiyama Y (2006) Expression and regulation of breast cancer resistance protein and multidrug resistance associated protein 2 in BALB/c mice. *Biol Pharm Bull* **29:**1032–1035.

Ho RH, Choi L, Lee W, Mayo G, Schwarz UI, Tirona RG, Bailey DG, Michael SC, and Kim RB (2007) Effect of drug transporter genotypes on pravastatin disposition in European- and African-American participants. *Pharmacogenet Genomics* **17:**647–656.

Ho RH and Kim RB (2005) Transporters and drug therapy: implications for drug disposition and disease. *Clin Pharmacol Ther* **78:**260–277.

Ho RH, Tirona RG, Leake BF, Glaeser H, Lee W, Lemke CJ, Wang Y, and Kim RB (2006) Drug and bile acid transporters in rosuvastatin hepatic uptake: function, expression, and pharmacogenetics. *Gastroenterology* **130:**1793–1806.

Hsiang B, Zhu Y, Wang Z, Wu Y, Sasseville V, Yang WP, and Kirchgessner TG (1999) A novel human hepatic organic anion transporting polypeptide (OATP2). Identification of a liver-specific human organic anion transporting polypeptide and

identification of rat and human hydroxymethylglutaryl-CoA reductase inhibitor transporters. *J Biol Chem* **274:**37161–37168.
Jonker JW, Wagenaar E, Mol CA, Buitelaar M, Koepsell H, Smit JW, and Schinkel AH (2001) Reduced hepatic uptake and intestinal excretion of organic cations in mice with a targeted disruption of the organic cation transporter 1 (Oct1 [Slc22a1]) gene. *Mol Cell Biol* **21:**5471–5477.
König J, Cui Y, Nies AT, and Keppler D (2000) A novel human organic anion transporting polypeptide localized to the basolateral hepatocyte membrane. *Am J Physiol Gastrointest Liver Physiol* **278:**G156–G164.
Marzolini C, Tirona RG, and Kim RB (2004) Pharmacogenomics of the OATP and OAT families. *Pharmacogenomics* **5:**273–282.
Nakai D, Nakagomi R, Furuta Y, Tokui T, Abe T, Ikeda T, and Nishimura K (2001) Human liver-specific organic anion transporter, LST-1, mediates uptake of pravastatin by human hepatocytes. *J Pharmacol Exp Ther* **297:**861–867.
Ogura K, Choudhuri S, and Klaassen CD (2000) Full-length CDNA cloning and genomic organization of the mouse liver-specific organic anion transporter-1 (lst-1). *Biochem Biophys Res Commun* **272:**563–570.
Schachter M (2005) Chemical, pharmacokinetic and pharmacodynamic properties of statins: an update. *Fundam Clin Pharmacol* **19:**117–125.
Shimizu M, Fuse K, Okudaira K, Nishigaki R, Maeda K, Kusuhara H, and Sugiyama Y (2005) Contribution of OATP (organic anion-transporting polypeptide) family transporters to the hepatic uptake of fexofenadine in humans. *Drug Metab Dispos* **33:**1477–1481.
Sweet DH, Miller DS, Pritchard JB, Fujiwara Y, Beier DR, and Nigam SK (2002) Impaired organic anion transport in kidney and choroid plexus of organic anion transporter 3 (Oat3 (Slc22a8)) knockout mice. *J Biol Chem* **277:**26934–26943.
Tirona RG and Kim RB (2007) Organic anion transporting polypeptides (OATPs), in *Drug Transporters* (You G and Morris ME eds) Wiley-VCH, New York.
Tirona RG, Leake BF, Wolkoff AW, and Kim RB (2003) Human organic anion transporting polypeptide-C (SLC21A6) is a major determinant of rifampin-mediated pregnane X receptor activation. *J Pharmacol Exp Ther* **304:**223–228.
Vavricka SR, Van MJ, Ha HR, Meier PJ, and Fattinger K (2002) Interactions of rifamycin SV and rifampicin with organic anion uptake systems of human liver. *Hepatology* **36:**164–172.
Wagner M, Fickert P, Zollner G, Fuchsbichler A, Silbert D, Tsybrovskyy O, Zatloukal K, Guo GL, Schuetz JD, Gonzalez FJ, et al. (2003) Role of farnesoid X receptor in determining hepatic ABC transporter expression and liver injury in bile duct-ligated mice. *Gastroenterology* **125:**825–838.
Wagner M, Halilbasic E, Marschall HU, Zollner G, Fickert P, Langner C, Zatloukal K, Denk H, and Trauner M (2005) CAR and PXR agonists stimulate hepatic bile acid and bilirubin detoxification and elimination pathways in mice. *Hepatology* **42:**420–430.
Zollner G, Wagner M, Moustafa T, Fickert P, Silbert D, Gumhold J, Fuchsbichler A, Halilbasic E, Denk H, Marschall HU, et al. (2006) Coordinated induction of bile acid detoxification and alternative elimination in mice: role of FXR-regulated organic solute transporter-alpha/beta in the adaptive response to bile acids. *Am J Physiol Gastrointest Liver Physiol* **290:**G923–G932.

Address correspondence to: Richard B. Kim, ALL-152 LHSC—University Hospital, 339 Windermere Road, London, Ontario, N6A 5A5, Canada. E-mail: richard.kim@lhsc.on.ca